Spring 5-1-2022

Calcium Ferrite as a Semiconductor for Microbially Assisted Photocatalytic Reduction of Carbon Dioxide

Lauren King
lauren.a.king@uconn.edu

Calcium Ferrite as a Semiconductor for Microbially Assisted Photocatalytic Reduction of Carbon Dioxide

Lauren King

Department of Civil and Environmental Engineering

Thesis in Environmental Engineering

Supervisor: Dr. Alexander Agrios

Advisor: Dr. Christine Kirchhoff

May 12, 2022

Abstract

The pressing issue of global climate change has been found to be attributed to the increasing concentration of greenhouse gases in the atmosphere, especially carbon dioxide. One mitigation idea to close the carbon loop is to utilize redox reactions and photocatalysis to reduce carbon dioxide to a useable fuel source, like methane or methanol. This thesis will study the possibility of using calcium ferrite as the semiconductor to perform photocatalytic reduction of carbon dioxide with the assistance of a microbial fuel cell, which will help minimize the energy required from sunlight photons. A calcium ferrite thin film was produced through the sol-gel synthesis method. This production method must be completed in a nitrogen glove box, so a compact, low-cost dip-coating machine was built with a linear actuator and Arduino microcontroller. Once the cell was produced, x-ray diffraction and scanning electron microscopy were used to characterize the crystalline structure of the film. Additionally, a potentiostat was used to test the cell's potential, which determines its ability to reduce carbon dioxide and other test molecules. In conclusion of this study, the benefits and limitations of this synthesis method will be discussed, along with the feasibility of using calcium ferrite as the semiconductor for microbially assisted photocatalytic reduction of carbon dioxide.

Acknowledgements

I would like to thank Dr. Alexander Agrios and Iram Sifat for all of their mentorship throughout the research and writing process, as well as Dr. Christine Kirchhoff who has provided support through my coursework and career planning. I am also grateful for my family and friends who inspire me to challenge myself and follow my passions.

Table of Contents

Introduction

Global natural carbon dioxide, CO_2, fluctuation for the last 800,000 years has been found to be between 180-300 ppm, but there has been a gradual increase in atmospheric CO_2 concentrations since the industrial revolution (Habisreutinger et al., 2013). This has led to CO_2 levels that often exceed this range in recent decades, while still continuing to increase. The phenomena of the greenhouse effect and climate change can be greatly attributed to this increase in carbon dioxide concentrations, therefore there is a high demand for technology to either minimize new CO_2 emissions or remove existing CO_2 from the atmosphere. The difficulty however is to manage those goals without compromising the high quality of life and industrialization that the world has become accustomed to. One proposed solution is to utilize redox reactions to reduce CO_2 and other organics to usable carbon fuels like methane (CH_4) or methanal (CH_3OH) (Huang et al., 2020). Theoretically, carbon dioxide could be reduced in this way through very high-energy light hitting the surface of certain materials that are exposed to the atmosphere. Unfortunately, the most feasible light source for this of course is sunlight, which for the majority lacks light energy at these high levels. To overcome this obstacle, a microbial fuel cell could be coupled with the photocatalytic cell, to supply electrons that are already at a high enough energy level to utilize the sunlight energy to reduce CO_2. The major advantages of large-scale systems like this would be that the fuels produced could be used without much alteration to current natural gas infrastructure, it creates a closed carbon loop, and provides a strategy to store "solar energy" (Habisreutinger et al., 2013). Figure 1 shows that in the near term it is more profitable for specialty chemical products, but there is likely profitability in some carbon fuels as products as there are more fossil fuel taxes and better technology (Bertheussen et al., 2019). This paper will provide details on the reduction of CO_2 by photocatalysis when paired with a microbial fuel cell, and a review of a low-cost method testing a potential semi-conductor material for the photocatalytic cell, calcium ferrite.

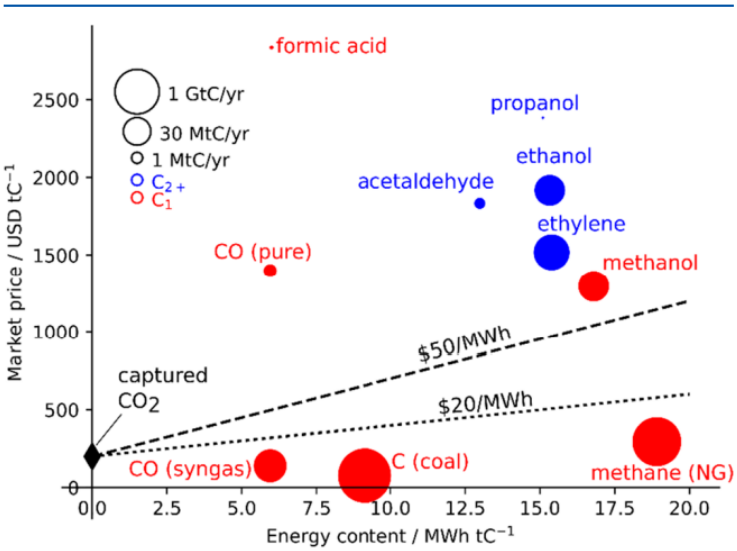

Figure 1: Market price of possible CO_2 reduction products as a function of energy content based on a CO_2 capture cost of $200/tC. Those above the $50 and $20 per MWh lines are more profitable than the average and minimum cost of energy currently produced by solar power, respectively. (Bertheussen et al., 2019)

Background

The goal of photocatalytic reduction of CO_2 is to convert it to a usable fuel source, like methane or methanol (Habisreutinger et al., 2013). This process begins with the absorption of sunlight, mainly visible light, and adsorption of a molecule, in this case CO_2, by a semiconductor surface. A diagram of this general process is shown in Figure 2. Semiconductors are differentiated by their bandgap, which is the difference in potential between the valence band (VB) and the conduction band (CB). If the photons absorbed from the light are at higher energy levels than the bandgap energy, they excite the electrons from the valence band to the conduction band. This creates holes in the valence band where the electrons were before, and they are considered virtually positively charged (Huang et al., 2020). The charge carriers, electrons and holes, may transfer to the adsorbed acceptor molecules which would initiate the reduction or oxidation reactions.

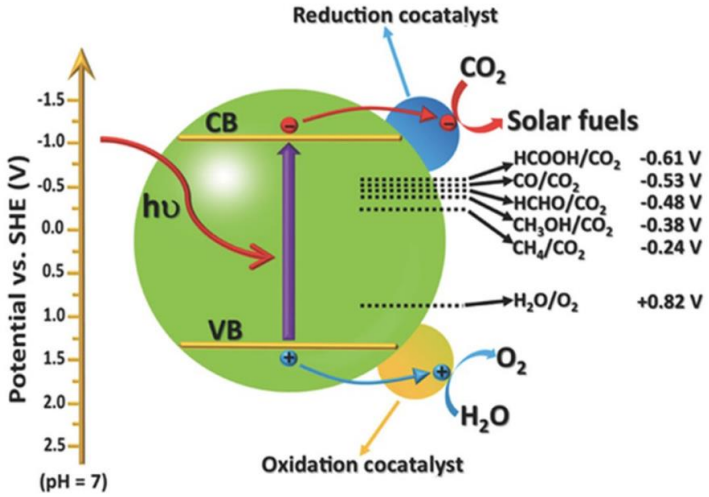

Figure 2: The general mechanism for photocatalytic reduction of CO_2 (Huang et al., 2020).

Reduction of a molecule would be easiest if only one electron is needed to facilitate the reduction, however CO_2 has a low electron affinity because of its symmetrical shape and closed-shell electron configuration, so it is very difficult to do a single electron reduction. Instead, the most plausible reductions use 2-8 electrons (Habisreutinger et al., 2013) depending on the desired product. More specifically, it requires 127 kcal/mol to break the carbon oxygen double bond of CO_2, leading to a relatively large potential of -1.9 V vs. NHE at pH 7 to reduce CO_2 with only one electron (Huang et al., 2020). This is avoided by using proton-assisted multi-electron processes which have potentials within more common ranges for semiconductors. In the past, this has mainly been done through thermal hydrogenation of CO_2, but electrochemical processes would be favored because it combines multiple steps into a single electrochemical process. This means that it can produce desired products more easily than the comparable thermal processes could, and even more importantly for scalability, it can often run at or near room temperature and pressure (Bertheussen et al., 2019).

$$CO_2 + e^- \rightarrow CO_2^{\cdot -} \quad E^0 = -1.90\,V \tag{1}$$

$$CO_2 + 2H^+ + 2e^- \rightarrow CO + H_2O \quad E^0 = -0.53\,V \tag{2}$$

$$CO_2 + 4H^+ + 4e^- \rightarrow HCHO + H_2O \quad E^0 = -0.48\,V \tag{3}$$

$$CO_2 + 6H^+ + 6e^- \rightarrow CH_3OH + H_2O \quad E^0 = -0.38\,V \tag{4}$$

$$CO_2 + 8H^+ + 8e^- \rightarrow CH_4 + 2H_2O \quad E^0 = -0.24\,V \tag{5}$$

$$2H_2O + 4h^+ \rightarrow O_2 + 4H^+ \quad E^0 = +0.81\,V \tag{6}$$

$$2H^+ + 2e^- \rightarrow H_2 \quad E^0 = -0.42\,V \tag{7}$$

Equations 1-7 show possible redox reactions, and their potentials, associated with the photocatalytic reduction of CO_2 (Huang et al., 2020).

For the photocatalytic reduction of CO_2, the semiconductor chosen should balance between being in the visible light range, which is fairly narrow, but the bandgap also needs to be large enough to cover the range of the reduction and oxidation potentials. Equations 1-7 show the associated potentials for various reduction pathways, revealing that all except the single electron process are less than the absolute value of -0.53 V (Habisreutinger et al., 2013). Furthermore, the semiconductor must actually have a higher voltage than the given potential for the desired redox reaction because of losses due to electrode overpotentials, resistivity, and charge transport (Tablero et al., 2017).

The semiconductor of interest in this paper is calcium ferrite, $CaFe_2O_4$, which has an orthorhombic structure, shown in Figure 3. Calcium ferrite has a conduction band of -0.6 V and a bandgap of 1.9 V. It is notable that this bandgap is equal to the potential for the reduction of CO_2 through the single electron process, and therefore it would not be feasible. However, this bandgap is significantly larger than the potentials for the multi-electron reductions of CO_2, so those reactions are feasible. Other advantages include that it has a high absorptivity of visible light, is made of abundant elements, and can be prepared at low cost (Chen et al., 2017). One downside of $CaFe_2O_4$ is that the valence band is approximately the same as the potential for the oxidation of water, so that reaction may not be possible as a couple for the reduction of CO_2 (Matsumoto et al., 1994).

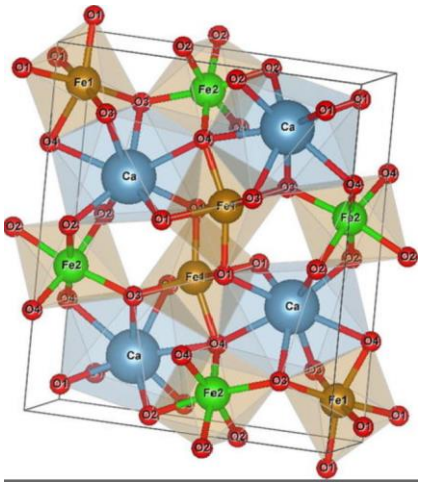

Figure 3: The structure of a unit cell of $CaFe_2O_4$ (Tablero et al., 2017).

To minimize the amount of energy needed to be supplied by sunlight for the photocatalytic reduction, the calcium ferrite cell will be coupled with a microbial fuel cell. Simply, there is an anode and cathode chamber, separated by a proton exchange membrane (PEM) (Adhami et al., 2015). In this system, the anode which performs oxidation, would be the side including microbes which can oxidize organic matter. This can be referred to overall as a bioanode-photocathode system, shown in Figure 4. The difference of potential between the two chambers moves bio-generated electrons to the valence band of the cathode, where they can then receive energy from sunlight photons (El-Gohary et al., 2022). The key feature of combining these systems becomes apparent here, since these transferred electrons will be at a higher energy than the ones coming from the cathode alone would be. This means that hopefully the sunlight can provide enough energy to boost them to the valence band, where they can perform reductions at higher potentials, like as needed for the reduction of CO_2.

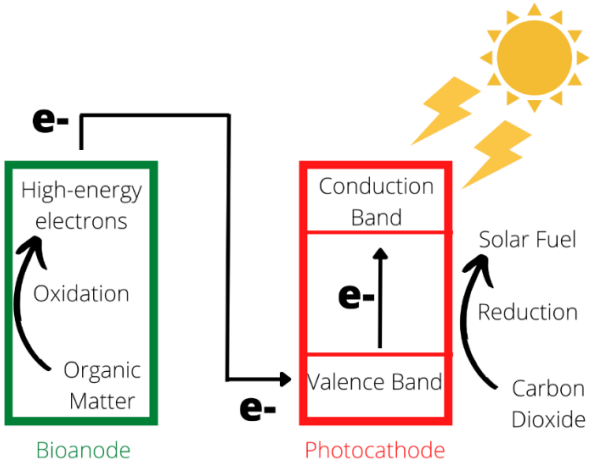

Figure 4: Bioanode-Photocathode system for reduction of CO_2.

Although this system is being designed for the reduction of CO_2, there are many reasons which make it difficult to test that reduction specifically through the development process. Carbon dioxide would have to be supplied to saturate the system, while oxygen would have to be removed. Additionally, carbon dioxide and carbonate compounds are naturally present in all aqueous solutions, so it is difficult to quantify and maintain a desired concentration. Furthermore, CO_2 is a reactant and a buffer in CO_2/bicarbonate system, which means if the redox reactions begin changing the pH on the cathode surface, the concentrations of CO_2 can begin being depleted as a buffer instead of as a reactant. The presence of oxygen in the system is also specifically harmful in testing this system because there is iron present in the stainless steel and film, meaning it can possibly lead to the oxidation of iron. This combined all leads to electrodes becoming less active and selective over time because of reaction intermediates that deposit on the surface and restructuring of the surface because of reaction conditions (Bertheussen et al., 2019). To avoid these issues and produce more reliable results as the film and cell is optimized, an organic molecule, methyl viologen (MV), was used instead in electrochemical testing as a probe for CO_2. The structure and expected cyclic voltammetry testing results of the MV ions are shown in Figure 5. The reduction of MV^{2+} to MV^{+} is a reasonable testing probe because it peaks at -0.78 V (Chen et al., 2019), which is within the range of most desired CO_2 reduction potentials.

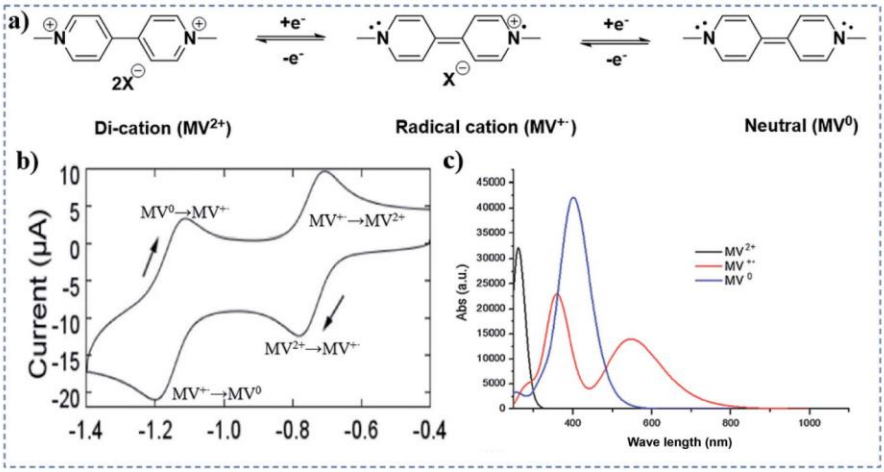

Figure 5: a) Structure of di-cation, radical cation, and neutral states of MV b) Expected cyclic voltammetry measurements of MV redox reactions c) Expected uv-vis absorption spectra of MV (Chen et al., 2019).

Additionally, reduction of methyl viologen occurs sequentially and reversibly from 2+ to + to neutral, and all states are thermodynamically stable which allows for consistent testing data. Lastly, during the radical cation, MV^{+} state it changes the surface of the electrode to an intense dark blue/purple color which makes it easy to observe (Chen et al., 2019), as can be seen in Figure 6.

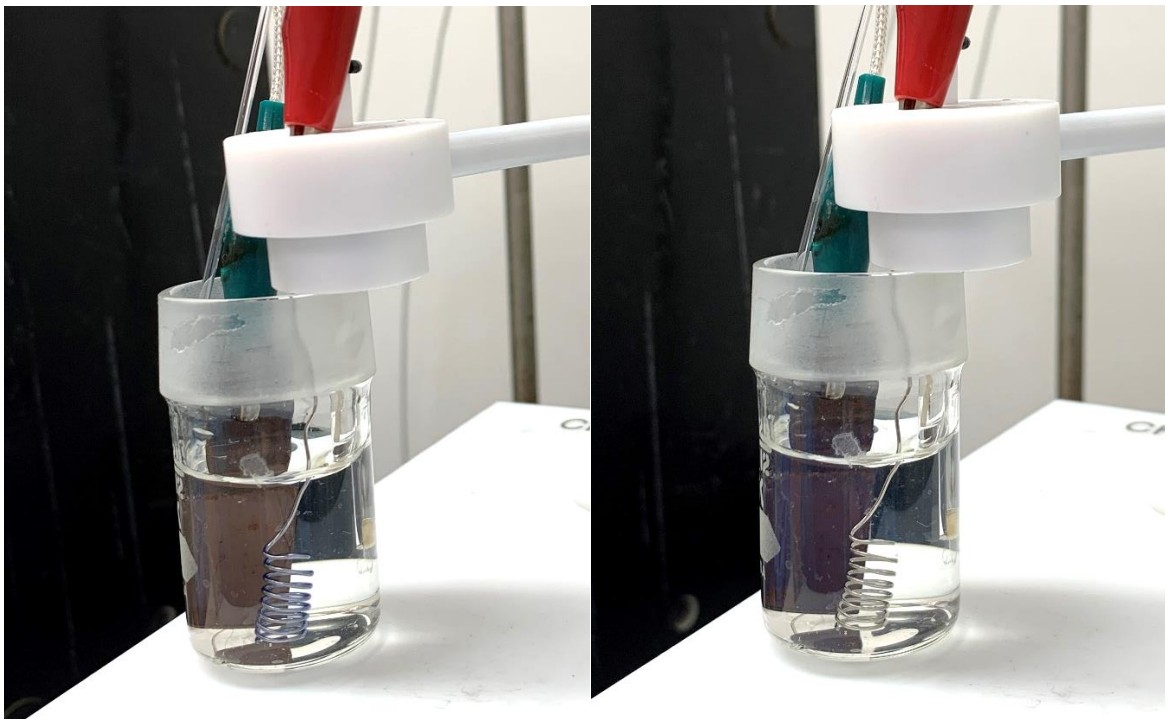

Figure 6: Left) MV in di-cation state, where working electrode slide is natural color Right) MV in radical cation state, showing intense blue/purple color on working electrode slide.

Methods

Dip-coating Robot

A small-size, low-cost dip-coating robot was built to perform the dip-coating at a specified speed. An Actuonix L12-R micro linear servo was utilized at a stroke length of 100 mm, gear ratio of 100:1, and voltage of 6V. It was controlled through an Arduino microcontroller and HC-05 Bluetooth module, as shown in Figure 7. A program was written in C++ to receive a 1 from PuTTY, a terminal emulator on a computer, to initiate the dip-coating and is shared in the dip-coating robot section of the Appendix.

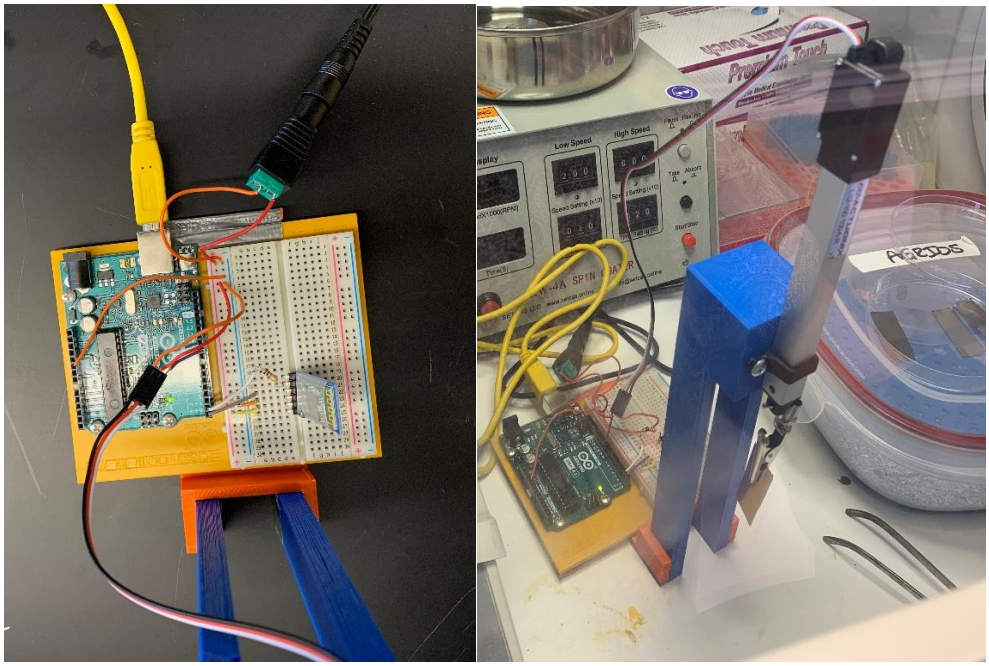

Figure 7: Wiring and set-up of dip-coating robot.

Calcium Ferrite Film Synthesis

A $CaFe_2O_4$ precursor solution was prepared in a 50 mL beaker through classical sol-gel synthesis. 661 mg of $Ca(NO_3)_2 \cdot 4H_2O$, 1,742 mg of $Fe(NO_3)_3 \cdot 9H_2O$, and 979 mg of block-copolymer poly(ethylene oxide)-*b*-poly(propylene oxide)-*b*-poly(ethylene oxide) were dissolved in 37 mL of ethanol and 13 mL of 2-methoxyethanol through ultrasonic treatment for 15 minutes. After ultrasonic treatment was complete, 10 mL of the solution was transferred to a 10 mL vial, and it was placed into a humidity-controlled glove box, at 10-15%, under the dip-coating machine. A 0.5 in x 1.5 in stainless steel slide was attached to the robot and was dip-coated with the calcium ferrite solution at a speed of 8 mm/s. The slide was left in place to allow it to dry in the chamber for 3 minutes. Next, the slide was immediately heated on a hotplate at 130°C within the glovebox for 1 hour. It was then transferred to a location with a muffle furnace, which was pre-heated to 130°C which the slide was then transferred into. The slide was heated at 130°C for 2 more hours, and then remained in the furnace as the temperature was increased to 300°C at a rate of 0.5°C/min. Lastly, the furnace was heated from 300°C to 700°C over one hour. The slide was heated in the furnace for 1 hour at 700°C and then was allowed to cool naturally.

Characterization

The crystalline structure of the calcium ferrite thin film was characterized by scanning electron microscopy (SEM) and x-ray diffraction (XRD). Electrochemical properties were tested through cyclic voltammetry with a potentiostat. 10 mL of the desired solution for that trial was first purged with Nitrogen for 15 minutes to remove any oxygen in the solution. Then the slide

was set in the solution as the working electrode, facing the reference electrode and counter electrode. The reference electrode used was stored in 4 M KCl and has a potential of approximately 0.2 V vs. SHE. A platinum spiral wire was used as the counter electrode. The combinations of working electrodes and solutions are diagramed in Figures 8-9. Each of these combinations was tested from 0 to -1 V at a sensitivity of 0.0003.

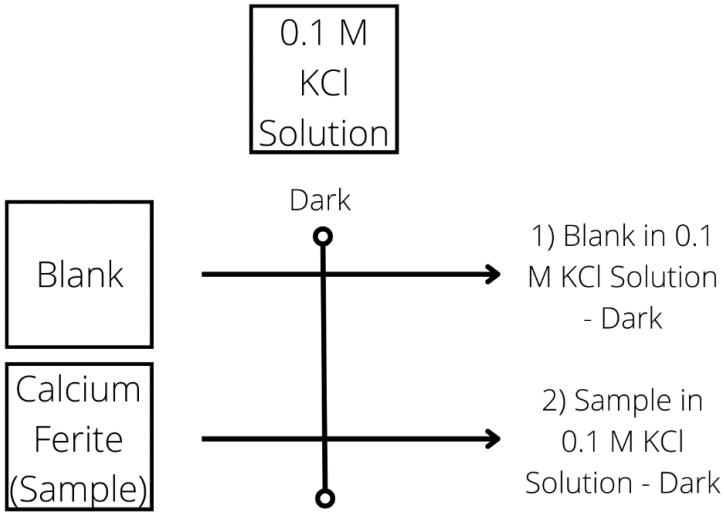

Figure 8: Trial conditions for 0.1 M KCl solution cyclic voltammetry.

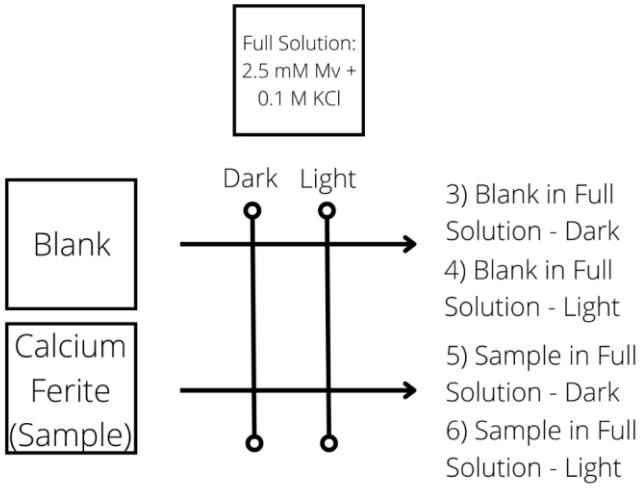

Figure 9: Trial conditions for full solution cyclic voltammetry.

Results

The first characterization method to verify the structure of the film was SEM. A blank slide was viewed and then analyzed in comparison to two slides with calcium ferrite films on

them. Firstly, the surface of the slides was viewed at different levels of magnification. Images were collected for each slide at a magnification of approximately 1000x. Since stainless steel already has a complex mix of elements, its surface structure is also significant, and therefore it is difficult to distinguish any major differences from the coated area images.

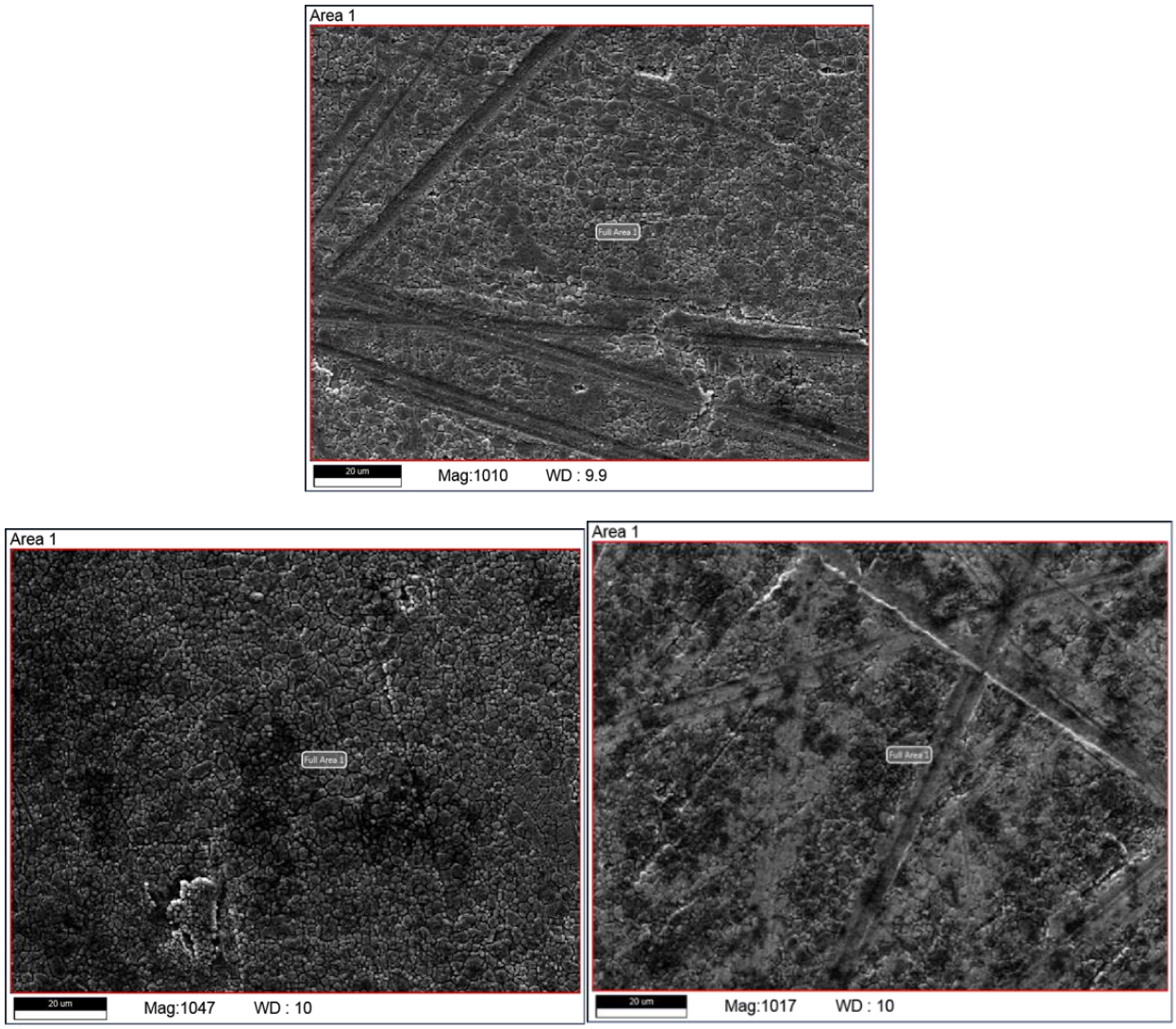

Figure 10: SEM image of Above) blank slide Left) D1 slide with $CaFe_2O_4$ film Right) D3 slide with $CaFe_2O_4$ film.

Although the surfaces are not visually different in a clear way, the images can be analyzed for the presence of individual elements. As mentioned above, stainless steel includes a variety of elements on its own, including iron, so it is expected that the presence of iron alone through analysis does not reveal much about the presence of the calcium ferrite film. All samples found the weight proportion of Fe in the sample to be about 60%. The notable element to find

would be calcium, however this was only found in one of the film samples, and at a weight of only 0.8%. This likely means that the presence of calcium on the other film sample was too small of a proportion to report in comparison to the array of other elements present, or it could possibly not be present at all.

Following the discovery of the presence of calcium and iron in the film, XRD was then used to determine if it was present in the correct crystalline structure. According to Kirchhberg et al., notable peaks for $CaFe_2O_4$ should be present at approximately, 33°, 35°, 41°, 43°, 50°, and 62°. The notable peaks found on the stainless steel slides through XRD were at 44°, 51°, and 75°. These peaks were consistent on the blank and calcium ferrite slides at similar intensities for all angles, as can be seen in Figure 11. According to XRD analysis of stainless steel substrates under different heating conditions by Cao et al., the peaks at approximately 50.5° and 75° are due to the stainless steel substrate. Furthermore, Cao et al. concluded that a peak around 45° is a result of tetragonal zirconia, which becomes stronger and sharper as temperature increases (Cao et al., 2001). Considering that the peaks through XRD testing were consistent between the blank and sample slide, and all notable peaks correspond with those that the literature deems are characteristic of stainless steel, it is unlikely that the calcium and iron have correctly formed a phase-pure, porous calcium ferrite thin film.

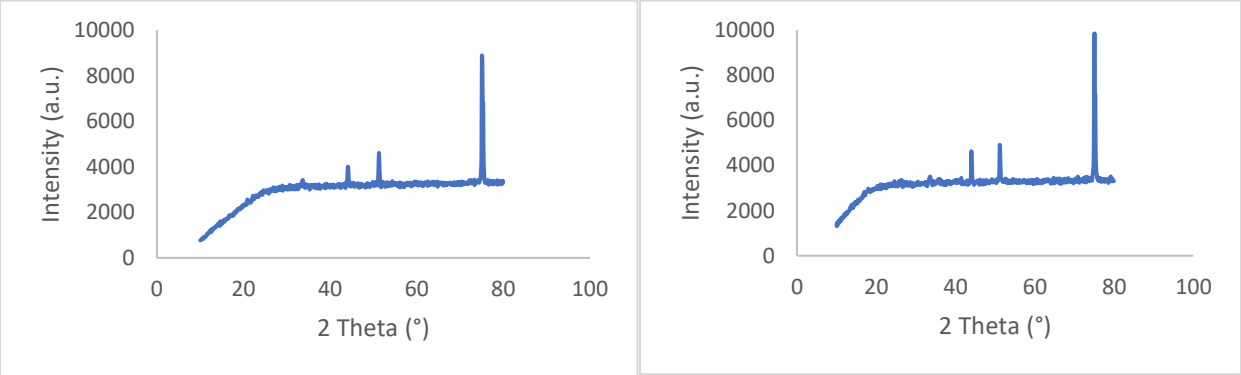

Figure 11: XRD results for Left) A blank stainless steel slide Right) A stainless steel slide with a $CaFe_2O_4$ film.

Although structure characterization reveals the presence of iron and calcium, it also points to either a lack of or minimal formation of calcium ferrite. Since the elements are present, photochemical testing was still conducted to find effects of the film on the reduction of MV^{2+}. First, cyclic voltammetry was conducted on a blank and sample slide in a KCl only solution to determine their curves based on only charging and uncharging the electrodes. There should not be any characteristic redox peaks within these trials since the MV^{2+} ions are not present. A vertical line at -0.78 V, the expected potential at which MV^{2+} is reduced to MV^{+} was place on each graph to clarify where the reduction peak is expected to maximize. Figure 12 shows that

neither the blank nor the sample slide, have any peak or unique behavior at this potential when there is no presence of MV^{2+} ions. Interestingly, the calcium ferrite slide has a wider base range of current across this voltage range.

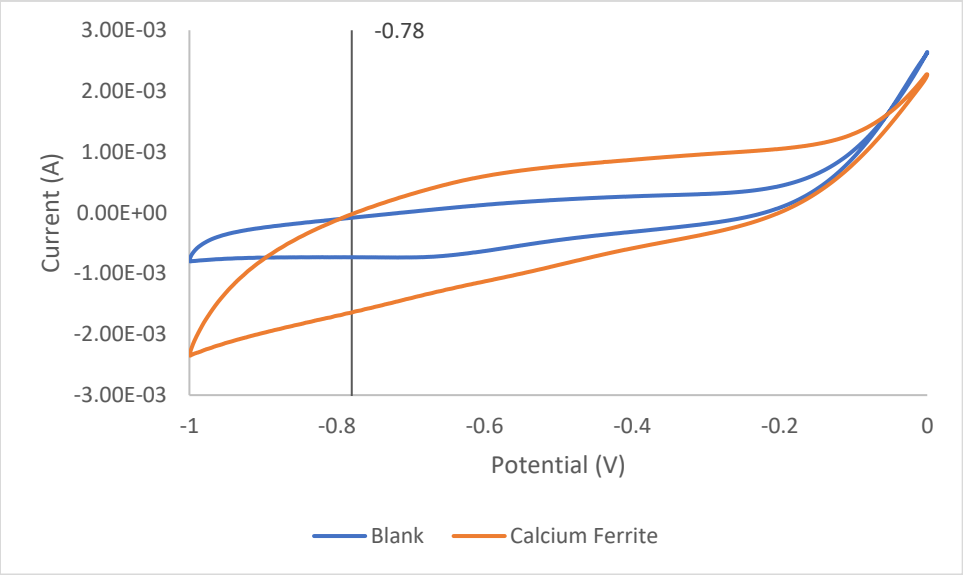

Figure 12: Cyclic voltammetry for trial conditions 1 and 2, a blank and sample slide in KCl only solution in the dark.

Next, the blank and calcium ferrite slides were measured in the full solution in dark and light conditions, shown in Figures 13-14. The second of three total cycles was used to represent each trial condition, and at the potential of interest, -0.78 V, the blank slide in the dark produced a current of -0.667 mA, while in the light it produced a current of -0.482 mA. This shows a decrease in the magnitude of the current from dark to light conditions of 27.8%. For the calcium ferrite slide in dark conditions it produced a current of -0.713 mA at -0.78 V, and -0.589 mA in light conditions. This corresponds to a 17.4% decrease in magnitude of the current produced at the potential needed for the reduction of MV^{2+}. However, for both the blank and sample slides, there was a consistent trend of decreasing magnitude of current as the cycle number increased, with a maximum at the first dark cycle and minimum at the last light cycle. Since current is proportional to the reaction rate, something is causing there to be less reduction of MV^{2+} over time, however it does not seem to be affecting the oxidation rate.

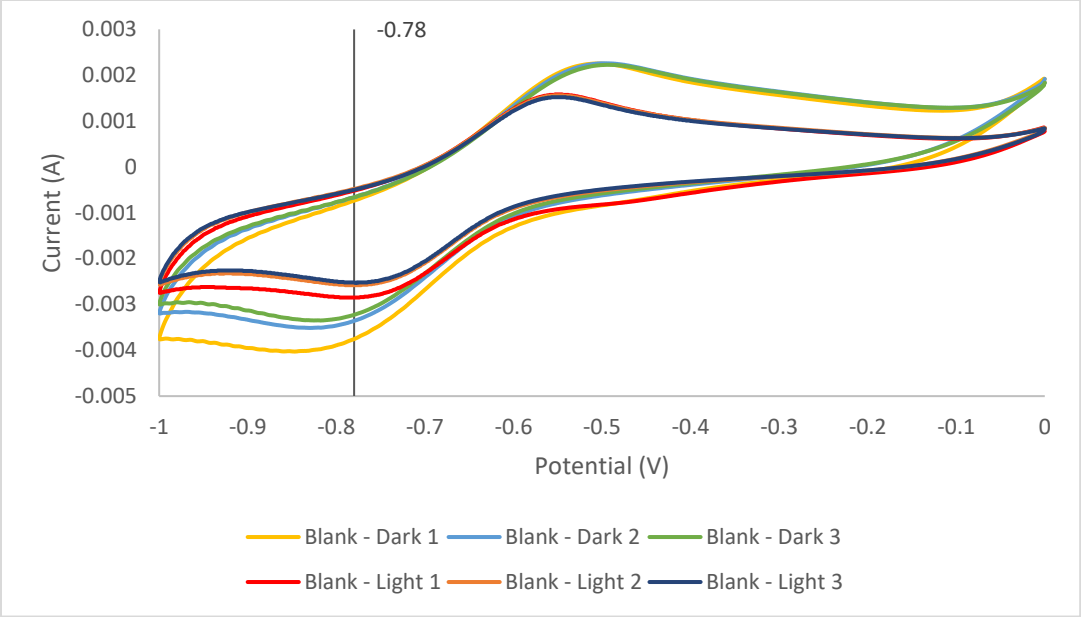

Figure 13: Cyclic voltammetry for trial conditions 3 and 4, a blank slide in the full solution in dark and light conditions.

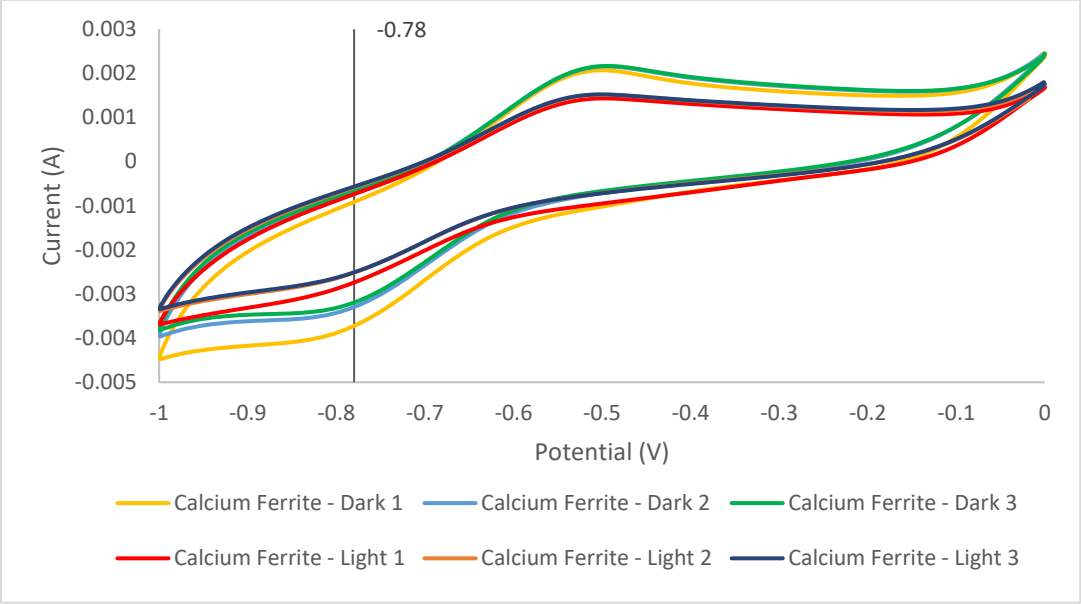

Figure 14: Cyclic voltammetry for trial conditions 5 and 6, a sample slide in the full solution in dark and light conditions.

Conclusion

Time constraints did not allow for further trials at this time, but based on the favorable semiconductor characteristics of calcium ferrite for CO_2 reduction, it should continue to be

considered in future research. Other methods for the synthesis of calcium ferrite solution may be more consistent for producing a significant concentration of calcium ferrite. Additionally, the Kirchhberg et al. method which was followed used indium tin oxide coated quartz glass slides which are very expensive, but may allow for a better film deposition than was possible on stainless steel. It is recommended to continue depositions on stainless steel and other low-cost substrates to find one most suitable for calcium ferrite films. On a larger scale, it is also recommended for further research into the actual pathway used for the reduction of carbon dioxide, because according to Habisreutinger et al. there are currently competing theories. This would lead to a better understanding of the specifications needed for the redox reactions to happen efficiently and effectively. Further testing could also be done to improve the efficiency of the reduction through reducing the bandgap of the semiconductor. Some possible options for this would be the addition of metal nanoparticles or a dopant.

Appendix

Dip-Coating Robot Program

```
#include <Servo.h>

Servo myservo; // create servo object to control a servo

int pos = 0; // stores servo position


#include "SoftwareSerial.h"

SoftwareSerial BTSerial(0, 1); //RX, TX


int act = 9;

int state = 1;


void setup() {
  myservo.attach(9); // attaches servo to pin 9
  pinMode(act, OUTPUT);
  BTSerial.begin(9600); // baud rate for bluetooth
}


void loop() {
```

```
 if(BTSerial.available()) { // checks if there's incoming data
  state = BTSerial.read(); // if there is then read the data and store in state
 }
 if(state == '0') {
  delay(10);
  for (int i = 0; i < 1; i++) {
   for (pos = 0; pos <=180; pos += 1) { // goes from 0 to 180 degrees in steps of 1 degree
    myservo.write(pos); // tell servo to go to position in variable 'pos'
    delay(130); // control speed
    state = 2;
   }
  }
  BTSerial.println("Extension Complete");
 }
 else if(state == '1') {
  delay(10);
  for (int n = 0; n < 1; n++) {
   for (pos = 180; pos >=0; pos -= 1) { // goes from 180 to 0 degrees in steps of 1 degree
    myservo.write(pos); // tell servo to go to position in variable 'pos'
    delay(130); // control speed
    state = 2;
   }
  }
  BTSerial.println("Retraction Complete");
 }
}
```

References

Adhami, A., Darvari, S., Oh, S., Rahimnejad, M., & Zirepour, A. (2015). Microbial fuel cell as new technology for bioelectricity generation: A review. *Alexandria Engineering Journal, 54.*(3), 745-756. https://doi.org/10.1016/j.aej.2015.03.031

Bertheussen, E., Chan, K., Chorkendorff, I., Engstfeld, A. K., Hahn, C., Horch, S., Jaramillo, T. F., Liu, X., Nitopi, S., Nørskov, J. K., Scott, S. B., Seger, B., & Stephens, I. E. L. (2019). Progress and Perspectives of Electrochemical CO_2 Reduction on Copper in Aqueous Electrolyte. *Chemical Reviews, 119.*(12), 7610-7672. http://dx.doi.org/10.1021/acs.chemrev.8b00705

Chen, Q.-Y., Zhang, K., Liu, J.-S., & Wang, Y.-H. (2017). Hydrogen and electricity production in a light-assisted microbial photoelectrochemical cell with CAFE2O4 photocathode. *Journal of Photonics for Energy*, *7*(2), 026501.

Cao, Y., Hu, X., Wang, X., & Yu, Y. (2001). Study on the structure and properties of ZrO_2 buffer layers on stainless steel by XRD, IR and AES. *Applied Surface Science, 172.(*3-4), 260-264. https://doi.org/10.1016/S0169-4332(00)00863-1

Chen, Y., Ding, J., Li, M., Lu, C., Wang, L., Zhai, G., Zheng, C., & Zhuang, X. (2019). Viologen-inspired functional materials: synthetic strategies and applications. *Journal of Materials Chemistry A, 7(*41), 23337-23360. https://doi.org/10.1039/C9TA01724K

El-Gohary, F., Mahmoud, M., Rafieenia, R., Rossa, C. A., & Sulonen, M. (2022). Integration of microbial electrochemical systems and photocatalysis for sustainable treatment of organic recalcitrant wastewaters: Main mechanisms, recent advances, and present prospects. *Science of The Total Environment, 824*, 153923. https://doi.org/10.1016/j.scitotenv.2022.153923

Habisreutinger, S. N., Schmidt-Mende, L., & Stolarczyk, J. K. (2013). Photocatalytic Reduction of CO2 on TiO2 and Other Semiconductors. *A Journal of the German Chemical Society, 52*(29), 7372–7408. https://doi.org/10.1002/anie.201207199

Huang, X., Gu, W., Ma, Y., Liu, D., Ding, N., Zhou, L., Lei, J., Wang, L., & Zhang, J. (2020). Recent advances of doped graphite carbon nitride for photocatalytic reduction of CO2: A Review. *Research on Chemical Intermediates*, *46*(12), 5133–5164. https://doi.org/10.1007/s11164-020-04278-6

Kirchberg, K., & Marschall, R. (2019). Low temperature synthesis of mesoporous CAFE2O4 photocathodes with hierarchical pore morphology. *Sustainable Energy & Fuels*, *3*(5), 1150–1153.

Matsumoto, Y., Obata, M., & Hombo, J. (1994). Photocatalytic reduction of carbon dioxide on P-type cafe2o4 powder. *The Journal of Physical Chemistry*, *98*(11), 2950–2951. https://doi.org/10.1021/j100062a035

Tablero, C. (2017). CaFe2O4 as a self-sufficient solar energy converter. *Journal of Applied Physics, 122*(13), 133114. https://doi.org/10.1063/1.4993537